RMetS
Royal Meteorological Society

# Comparison of Lorenz and Charney–Phillips vertical discretisations for dynamics–boundary layer coupling. Part I: Steady states

D. Holdaway,[a,b,c]* J. Thuburn[a] and N. Wood[d]‡

[a]*College of Engineering, Mathematics and Physical Sciences, University of Exeter, UK*
[b]*Goddard Earth Sciences Technology and Research, Universities Space Research Association, MD, USA*
[c]*Global Modeling and Assimilation Office, NASA Goddard Space Flight Center, MD, USA*
[d]*Met Office, Exeter, UK*

*Correspondence to: D. Holdaway, Code 610.1, Goddard Space Flight Center, Greenbelt, MD 20771, USA.
E-mail: dan.holdaway@nasa.gov
‡The contribution of this author was written in the course of his employment at the Met Office, UK, and is published with the permission of the Controller of HMSO and the Queen's Printer for Scotland.

**Accurate coupling between the resolved-scale dynamics and the parametrised physics is essential for accurate modelling of the atmosphere. Previous emphasis has been on the temporal aspects of this so-called physics–dynamics coupling problem, with little attention on the spatial aspects. When designing a model for numerical weather prediction there is a choice for how to vertically arrange the predicted variables, namely the Lorenz and Charney–Phillips grids, and there is ongoing debate as to which is the optimal. The Charney–Phillips grid is considered good for capturing the potential vorticity dynamics and wave propagation, whereas the Lorenz grid is more suitable for conservation. However the Lorenz grid supports a computational mode. It is argued here that the Lorenz grid is preferred for modelling the stably stratified boundary layer. This presents the question: which grid will produce more accurate results when coupling the large-scale dynamics to the stably stratified planetary boundary layer? The question is addressed by examining the ability of both the Lorenz and Charney–Phillips grids to capture the steady state of a set of equations that simultaneously represents both large-scale dynamics and the planetary boundary layer. The results show that the Charney–Phillips grid is able to capture accurately the steady boundary-layer solution provided the Richardson number is calculated without vertically averaging the shear. Averaging the shear suppresses the negative feedback of the shear on the diffusion coefficient; the positive feedback, via the vertical gradient of potential temperature, then leads to the formation of unrealistic step-like features.** **Copyright © 2012 Royal Meteorological Society**

*Key Words:* physics–dynamics coupling; steady-state boundary layer; vertical staggering; NWP

*Received 27 March 2012; Revised 15 June 2012; Accepted 9 July 2012; Published online in Wiley Online Library 21 September 2012*

*Citation:* Holdaway D, Thuburn J, Wood N. 2013. Comparison of Lorenz and Charney–Phillips vertical discretisations for dynamics–boundary layer coupling. Part I: Steady states. *Q. J. R. Meteorol. Soc.* **139**: 1073–1086. DOI:10.1002/qj.2016

## 1. Introduction

An important challenge in numerical weather and climate prediction is to obtain accurate coupling between models formulated for the parametrised physics and the models formulated for resolved large-scale dynamics. This is a difficult problem due to the wide range of both spatial scales and temporal scales supported.

A number of authors have considered the appropriate time-stepping scheme for the coupled problem (Wedi, 1999; Staniforth *et al.*, 2002a,b; Williamson, 2002; Cullen and Salmond, 2003; Dubal *et al.*, 2004, 2005, 2006). However, so far little emphasis has been placed on the spatial aspects of this so-called physics–dynamics coupling problem. This article addresses the vertical spatial aspects for coupling large-scale dynamics to an eddy viscosity model of the planetary boundary layer.

There is considerable choice for how to construct the model in space, namely the three connected issues of vertical coordinate system, choice of predicted variable and variable arrangement. The vertical coordinate may be chosen from, among others, height-based, mass-based or pressure-based. For a fully compressible system, the variables required in order to obtain a closed calculation of the governing equations include the three components of velocity and two thermodynamic variables. The two thermodynamic variables can be chosen from, for example, potential temperature, temperature, pressure, density or entropy. The arrangement of the variables divides into choice of horizontal staggering and choice of vertical staggering. In order to minimise spatial averaging of terms in the governing equations, it may be beneficial to store model variables at different places in space. Examples of the horizontal staggering include the classic Arakawa A- to E-grids (Arakawa and Lamb, 1977). Popular in atmospheric modelling, due to good representation of the dispersion relation, and in operational use at the Met Office (Davies *et al.*, 2005), is the C-grid. In the vertical there are two common choices of staggering, the Lorenz grid (Lorenz, 1960) and the Charney–Phillips grid (Charney and Phillips, 1953). The configuration of variables for these grids are shown in Figure 1. There is ongoing debate as to which staggering is the best option; for example the Met Office now employs the Charney–Phillips configuration (Davies *et al.*, 2005) whereas the European Centre for Medium-range Weather Forecasts (ECMWF) uses a variation of the Lorenz configuration (Beljaars, 1992; Untch and Hortal, 2004). These issues of spatial arrangement are inextricably connected with each other. For a particular vertical coordinate, it may be preferable to use certain thermodynamic variables and as a result a certain grid staggering.

Considering the breadth of choice available, it is possible that some heuristic argument could be applied, based on the features that a model should be capable of capturing, in order to make a decision on how to spatially construct a model. However, the issue here is that the full equation set is highly complex and so differences between two rival configurations may not be immediately apparent or clear-cut. In order to address the question for the 'dynamics only' case, Thuburn and Woollings (2005) constructed 168 test cases covering three types of vertical coordinate, every combination of two from a choice of five thermodynamic variables and a number of different vertical staggerings, including the Lorenz and Charney–Phillips grids. Thuburn and Woollings (2005) concentrated on the vertical configuration; the horizontal staggering has been well studied (e.g. Fox-Rabinovitz, 1994). The methodology used was one of normal mode analysis, to allow systematic checking of every combination and to grade any configuration from optimal to problematic based on its ability to represent the dispersion relation. For the height-based and mass-based coordinate, the optimal configurations are those which have pressure and potential temperature as the thermodynamic variables and use the Charney–Phillips grid for the arrangement of variables. It was later identified that, when using the Exner form of pressure gradient, density can be used in place of pressure as a prognostic variable whilst retaining optimal representation of the dispersion relation (Thuburn, 2006; Toy and Randall, 2007). For the same vertical coordinate and choice of thermodynamic variables that is optimal when using the Charney–Phillips grid, the Lorenz grid is only near-optimal; it gives quite good dispersive properties but supports a zero frequency computational mode (Schneider, 1987; Arakawa and Moorthi, 1988; Hollingsworth, 1995; Arakawa and Konor, 1996; Cullen *et al.*, 1997). The computational mode is a spurious solution resulting from having one too many degrees of freedom; it can interact with other modes and reduce overall accuracy. On the other hand, the Lorenz grid provides a cleaner route to ensuring conservation of energy than the Charney–Phillips grid.

The work of Thuburn and Woollings (2005) was for the inviscid case, i.e. one where only the resolved-scale dynamics are captured in the model but without any physics. Different conclusions may be reached regarding optimal vertical configuration when physics are included in the equations. Thuburn and Woollings (2005) show the Charney–Phillips grid to give the optimal configuration for the dynamics, however it is likely (section 3) that the Lorenz grid will offer the most accurate representation of the stably stratified boundary-layer parametrisation (e.g. Cullen *et al.*, 1997). In addition to the conflict that arises when modelling physics and dynamics separately, it is not clear how the coupling will influence the choice of configuration. The boundary layer will likely distort certain features of the dynamics, for example. An important question here is what happens to the computational mode. For example, suppression of the computational mode by the boundary layer would be of significant benefit to the Lorenz grid. This question is addressed in the second part of this study (Holdaway *et al.*, 2012, hereafter Part II).

Given the apparent conflict that arises between the dynamics-only case and the boundary layer-only case, the coupled version provides an interesting way to develop some understanding of the spatial aspects of the physics–dynamics coupling, particularly the choice of Lorenz or Charney–Phillips grid.

A popular method for comparing competing numerical configurations, and seen in a number of studies (e.g. Arakawa and Konor, 1996; Zhu and Smith, 2003) relies on examination of model output after simulations with the competing configurations. Although this technique provides useful testing methodologies, it does not offer particularly general results. A more systematic methodology that also allows for more general conclusions involves expanding the system into its steady and time-dependent (transient) parts and examining the two separately; this is the methodology used by Thuburn and Woollings (2005). Examining the

 

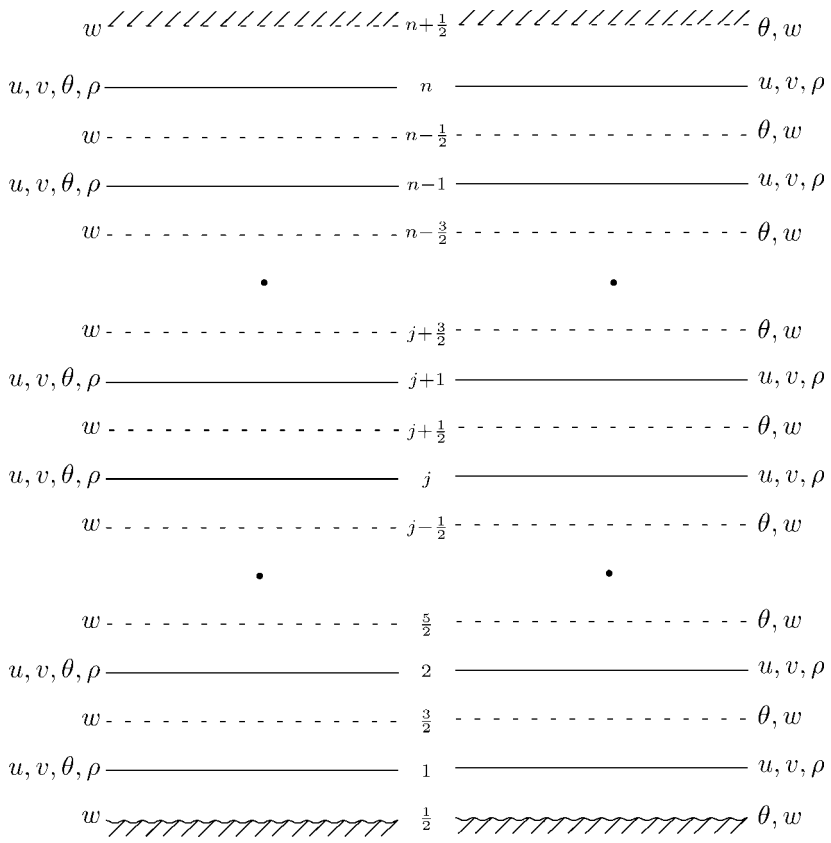


**Figure 1.** Lorenz (left) and Charney–Phillips (right) configurations of model variables. Dashed lines denote the half levels and solid lines denote the full levels.

steady state first allows one to examine the overall structure of the solution and identify any particularly problematic configurations. The transient part of the solution can be examined by studying the modes of variability (Part II). This methodology enables the study of the individual scales of motion supported by the time-dependent equations and so reveals why differences between particular configurations arise.

Despite the simplifications afforded by eliminating the time-dependent terms in the equations, it is shown below that examination of the steady state is non-trivial. Complexity in the equations results in difficulty obtaining good convergence properties. Further, additional terms are required in order to produce a realistic potential temperature profile. Part I examines the methodology that is required to examine the steady state and presents a comparison of the ability of the Lorenz and Charney–Phillips grids for capturing the steady state. The methodology required to examine the transients is also non-trivial to apply. This methodology, as well as results of the comparison, are presented in Part II of this study.

Part I is arranged as follows: section 2 outlines the equation set which will be used to simultaneously capture the boundary layer and dynamics. Section 3 provides discussion of the Lorenz and Charney–Phillips grids and why a conflict arises in which grid will be optimal. Section 4 outlines the equations required for obtaining a steady state of the problem. Section 5 compares the use of the Lorenz and Charney–Phillips grids for computing the steady state for the boundary layer together with the dynamics, and for the boundary layer on its own. Section 6 offers some concluding remarks.

## 2. Equations for modelling the dynamics and stably stratified boundary layer

A popular method for modelling turbulence in the atmospheric boundary layer is Reynolds averaging. The fully compressible Reynolds-averaged Navier–Stokes (RANS) equations (Tannehill *et al.*, 1997) capture the large-scale mean properties of the flow; turbulence on the mean flow is represented through Reynolds stresses. For the boundary layer, some of these Reynolds stresses are negligible; the RANS equations that have sufficient stress terms for capturing the stably stratified atmospheric boundary layer are (Holton, 2004)

$$\frac{\mathrm{D}u}{\mathrm{D}t} - fv + c_p\theta\frac{\partial\pi}{\partial x} = -\frac{1}{\rho}\frac{\partial}{\partial z}\left(\rho\overline{u''w''}\right), \quad (1)$$

$$\frac{\mathrm{D}v}{\mathrm{D}t} + fu + c_p\theta\frac{\partial\pi}{\partial y} = -\frac{1}{\rho}\frac{\partial}{\partial z}\left(\rho\overline{v''w''}\right), \quad (2)$$

$$\frac{\mathrm{D}w}{\mathrm{D}t} + c_p\theta\frac{\partial\pi}{\partial z} = -g, \quad (3)$$

$$\frac{\mathrm{D}\theta}{\mathrm{D}t} = -\frac{1}{\rho}\frac{\partial}{\partial z}\left(\rho\overline{\theta''w''}\right), \quad (4)$$

$$\frac{\mathrm{D}\rho}{\mathrm{D}t} + \rho\left(\frac{\partial u}{\partial x} + \frac{\partial v}{\partial y} + \frac{\partial w}{\partial z}\right) = 0, \quad (5)$$

where

$$\frac{\mathrm{D}}{\mathrm{D}t} = \frac{\partial}{\partial t} + u\frac{\partial}{\partial x} + v\frac{\partial}{\partial y} + w\frac{\partial}{\partial z}. \quad (6)$$

The constant $f = 1.031\times10^{-4}\mathrm{s}^{-1}$ is the Coriolis parameter. Terms on the right-hand side in Eqs (1), (2) and (4) are

 

Reynolds stresses; the double prime notation is used to note that Reynolds averaging is mass-weighted and that the system is compressible. Thermodynamic variables are related through the ideal gas law,

$$p = R\theta \left(\frac{p_0}{p}\right)^{-\kappa_g} \rho. \tag{7}$$

Exner pressure and standard pressure are related by

$$\pi = \left(\frac{p}{p_0}\right)^{\kappa_g}. \tag{8}$$

The constant $\kappa_g = R/c_p$, where $c_p = 1005.0\,\mathrm{J\,kg^{-1}K^{-1}}$ is the specific heat capacity for dry air and $R = 287.05\,\mathrm{J\,kg^{-1}K^{-1}}$ is the gas constant for dry air.

Note that the Exner form of pressure gradient is used. This is in keeping with the findings of Thuburn (2006) and Toy and Randall (2007), where it is shown that use of $c_p\theta\nabla\pi$ rather than $(1/\rho)\,\nabla p$ provides a straightforward way to ensure optimality while having density as a prognostic variable. For the study here, the predicted variables are thus the three components of velocity $u$, $v$ and $w$, potential temperature $\theta$ and density $\rho$. The vertical coordinate will be height-based.

### 2.1. Stress closure

Reynolds averaging results in stresses, which are unknown in terms of the predicted mean part of the flow. In order to write stresses in terms of the predicted variables, a closure and a parametrisation are required. The closure that is used here is the $K$-closure for stable boundary layers of Louis (1979),

$$-\overline{u''w''} = \tau_x = K_\mathrm{m}\frac{\partial u}{\partial z}, \tag{9}$$

$$-\overline{v''w''} = \tau_y = K_\mathrm{m}\frac{\partial v}{\partial z}, \tag{10}$$

$$-\overline{\theta''w''} = \mathcal{H} = K_\mathrm{h}\frac{\partial \theta}{\partial z}. \tag{11}$$

Eddy viscosity $K_\mathrm{m}$ and eddy heat diffusivity $K_\mathrm{h}$ are parametrised as

$$(K_\mathrm{m}, K_\mathrm{h}) = l^2\left|\frac{\partial \mathbf{u}}{\partial z}\right|\{f_\mathrm{m}(Ri), f_\mathrm{h}(Ri)\}, \tag{12}$$

where $\mathbf{u}$ is the velocity vector and $|\partial\mathbf{u}/\partial z| = \left[(\partial u/\partial z)^2 + (\partial v/\partial z)^2\right]^{1/2}$ is the wind shear. The mixing length is

$$l = \frac{\kappa z l_\infty}{\kappa z + l_\infty}, \tag{13}$$

where neutral mixing length is $l_\infty = 20$ m and $\kappa = 0.4$ is the von Kármán constant. The stability functions that are used are the SHARP form of King *et al.* (2001),

$$\{f_\mathrm{m}, f_\mathrm{h}\} = \begin{cases} a\left(\frac{1}{20Ri}\right)^2 & \text{for } Ri \geq 0.1, \\ a(1-5Ri)^2 & \text{for } 0 \leq Ri < 0.1, \end{cases} \tag{14}$$

where $a = 1$ for $f_\mathrm{m}$ and $a = 1/Pr$ for $f_\mathrm{h}$. The Prandtl number $Pr$ is a ratio of kinematic viscosity and heat diffusivity, i.e. $K_\mathrm{m}/K_\mathrm{h}$; here the neutral value is used $Pr = 0.7$. Richardson number is the ratio between buoyancy frequency and shear,

$$Ri = g\frac{\partial \ln(\theta)}{\partial z}\Big/\left|\frac{\partial \mathbf{u}}{\partial z}\right|^2. \tag{15}$$

Near the surface a constant flux layer is assumed, and the equivalent bulk Richardson formulation is used:

$$\tau_{x0} = C_\mathrm{m} u, \tag{16}$$

$$\tau_{y0} = C_\mathrm{m} v, \tag{17}$$

$$\mathcal{H}_0 = C_\mathrm{h}(\theta - \theta_s). \tag{18}$$

$C_\mathrm{m} = C_\mathrm{mn}|\mathbf{u}|f_\mathrm{m}(Ri_\mathrm{b})$ and $C_\mathrm{h} = C_\mathrm{hn}|\mathbf{u}|f_\mathrm{h}(Ri_\mathrm{b})$, where $|\mathbf{u}| = \left(u^2+v^2\right)^{1/2}$, are known as the drag coefficients and are found by making use of the logarithmic structure as $z \to 0$ in Eqs (9)–(11). $\theta_s$ is the potential temperature at the height of the roughness length. The neutral drag coefficients are given by

$$C_{\{mn,hn\}} = \left[\kappa\Big/\ln\left(\frac{z}{z_{\{\mathrm{rm,rh}\}}}\right)\right]^2, \tag{19}$$

where $z_\mathrm{rm}$ and $z_\mathrm{rh}$ are the roughness lengths for momentum and heat; both will be taken to be 0.1 m. For ease of notation, both will be referred to as $z_\mathrm{r}$. The bulk Richardson number is given by

$$Ri_\mathrm{b} = g(z - z_\mathrm{r})\frac{(\ln\theta - \ln\theta_s)}{|\mathbf{u}|}. \tag{20}$$

## 3. Lorenz and Charney–Phillips grid staggering

The predicted variables are velocities, potential temperature and density. A number of issues restrict the placement of the predicted variables in the vertical. Firstly, to avoid averaging in Coriolis terms it is important to store the horizontal components of velocity at equivalent model levels. Secondly, staggering density with $u$ and $v$ and relative to $w$ ensures no vertical averaging is required in $\nabla\cdot\mathbf{u}$, making mass conservation more accurate. Finally storing $w$ at the domain edges makes fulfilling the no-flux boundary conditions accurate. This leaves $w$ lying at what are referred to here as the half levels and $u$, $v$ and $\rho$ lying together at the full levels. The difference between the Lorenz and Charney–Phillips grids is in the placement of potential temperature $\theta$, either at the half levels (Charney–Phillips) or at the full levels (Lorenz). The two grid-staggering configurations are shown in Figure 1. Full levels are referred to as $z_\rho$ levels and half levels are referred to as $z_w$ levels.

When the gradient of a variable is required at the same level as where that variable is stored, it must be averaged (equivalent to differencing over two times the grid spacing), and this introduces an inaccuracy. That the Charney–Phillips grid is most suitable for modelling the dynamics is due to the reduced number of times a differencing over two times the grid spacing is required in the discretised versions of Eqs (3) and (4) (without the Reynolds stress terms) compared with when using the Lorenz grid. As shown by Thuburn and Woollings (2005), averaging of $\theta$ in these equations leads to slowing of either inertio-gravity or Rossby modes, depending on the horizontal scale; with the Charney–Phillips grid no averaging is required. Further, consider the $c_p\theta\,(\partial\pi/\partial z)$ term

in Eq. (3). A wave in potential temperature with vertical wavelength approaching the vertical grid scale would be seriously deformed by the Lorenz grid averaging; if it were a two-grid wave (a wave with wavelength exactly twice the vertical grid spacing) the averaging would cause the wave to become invisible to the model; this is how the computational mode manifests itself, discussed further in Part II.

It is clear that using the Lorenz grid will introduce inaccuracy for the dynamics. However, consider the discretised version of Eq. (15). If using the Lorenz grid, then the Richardson number and all other terms in the boundary-layer closure are automatically computed at the required vertical level; if using the Charney–Phillips grid then some averaging has to occur in the Richardson number. It is therefore likely that the Lorenz grid will offer better representation of the stably stratified boundary layer and its associated processes.

### 3.1. *Charney–Phillips configurations*

When the Charney–Phillips grid is used, the horizontal velocity is staggered relative to potential temperature. $K_\mathrm{m}$ is required at the half levels and $K_\mathrm{h}$ is required at the full levels. Some averaging will be required and there are a number of different ways of obtaining $K_\mathrm{m}$ and $K_\mathrm{h}$. Firstly, note that the Richardson number can be computed at either full or half levels by averaging either shear or potential temperature gradient respectively; alternatively Richardson number could be computed at all model levels by averaging both.

In the cases where Richardson number is computed at either half or full levels, either $K_\mathrm{m}$ or $K_\mathrm{h}$, respectively, is immediately obtained at the correct level; however a further averaging is required to find the other. For example, if potential temperature gradient is averaged then Richardson number is found at the half levels $z_w$; this gives $K_\mathrm{m}$ where it is required but not $K_\mathrm{h}$. In order to obtain $K_\mathrm{h}$ at the full levels, $z_\rho$, one can average either $K_\mathrm{h}$ itself, the Richardson number or the stability function.

In the case where shear is averaged so that Richardson number is computed at the full levels, a further set of options arise for that averaging. For example, in the Richardson number it is shear squared that is required; one can either 'average then square' or 'square then average'.

To summarise: with the Charney–Phillips grid the boundary-layer terms can be found as:

I. Potential temperature gradient is averaged so that Richardson number is calculated at the $z_w$ levels.
II. Shear is averaged so that Richardson number is calculated the $z_\rho$ levels.
III. Both quantities are averaged so that Richardson number is computed at $z_\rho$ and $z_w$ grid levels.

For options II and III, where shear is averaged, another three options occur:

a. Average velocity gradients then square them in order to compute the squared modulus:

$$\left|\frac{\partial \mathbf{u}}{\partial z}\right|^2 = \left(\overline{\frac{\partial u}{\partial z}}\right)^2 + \left(\overline{\frac{\partial v}{\partial z}}\right)^2. \qquad (21)$$

b. Compute the modulus and then average before squaring:

$$\left|\frac{\partial \mathbf{u}}{\partial z}\right|^2 = \left\{\overline{\left[\left(\frac{\partial u}{\partial z}\right)^2 + \left(\frac{\partial v}{\partial z}\right)^2\right]^{1/2}}\right\}^2. \qquad (22)$$

c. Compute the squared modulus and then average:

$$\left|\frac{\partial \mathbf{u}}{\partial z}\right|^2 = \overline{\left[\left(\frac{\partial u}{\partial z}\right)^2 + \left(\frac{\partial v}{\partial z}\right)^2\right]}. \qquad (23)$$

For options I and II, the Richardson number is computed at either half or full levels and three options arise for how to find either $K_\mathrm{h}$ (option I) or $K_\mathrm{m}$ (option II).

i. $K_\mathrm{m}$ or $K_\mathrm{h}$ themselves can be averaged.
ii. The stability functions $f_\mathrm{m}(Ri)$ or $f_\mathrm{h}(Ri)$ can be averaged.
iii. The Richardson number $Ri$ can be averaged.

Configurations are labelled as, for example, II(b)-i, meaning Richardson number is found at full levels; in finding shear squared the averaged modulus is found before being squared and then $K_\mathrm{m}$ itself is averaged from the full to the half levels. The options for averaging presented above do not represent an exhaustive set but have been selected to demonstrate key results.

When using the Charney–Phillips grid with any of the above configurations, averaging is also required in the bulk formulation that is required at the lowest model levels. In Eqs (16)–(20), $u$, $v$ and $\theta$ are required at the same level; $\theta$ must be averaged to the lowest $z_\rho$ level to compute $\tau_0$, and $u$ and $v$ must be averaged to the second-lowest $z_w$ level to compute $\mathcal{H}_0$. Since the velocities and potential temperature are known to scale logarithmically near the surface, a straightforward averaging will likely be inaccurate. A more accurate result can be obtained by making use of the scaling; for example $u$ at the $z_{3/2}$ level can be obtained using

$$\overline{u}_{3/2} = \frac{\ln\left(\frac{z_{3/2}}{z_\mathrm{r}}\right)}{\ln\left(\frac{z_1}{z_\mathrm{r}}\right)} u_1. \qquad (24)$$

### 3.2. *Grid spacing*

In order to capture surface interaction, all operational atmospheric models employ a stretched grid with finer resolution near the ground.

For the testing performed here, low- and high-resolution grids will be required. The height of the domain is chosen as $d = 2$ km so as to concentrate on the interface between the boundary layer and dynamics. For the low-resolution grid, the number of grid points is $n = 10$, and for the high-resolution grid $n = 100$. The low-resolution model levels are taken from over the sea in a previous version of the Met Office global model that had 38 model levels. The $z_w$ half-levels are 0.1, 20.1, 80.1, 180.1, 320.1, 500.1, 720.1, 980.1, 1280.1, 1620.1 and 2000 m, giving $\Delta z$ spacings of 20, 60, 100, 140, 180, 220, 260, 300, 340 and 379.9 m. The $z_\rho$ full levels are 10.1, 50.1, 130.1, 250.1, 410.1, 610.1, 850.1, 1130.1, 1450.1, and 1810.1 m, giving $\Delta z_h$ spacings of 40, 80, 120, 160, 200, 240, 280, 320 and 360 m. The addition of 0.1 to each model level is due to the roughness length. There are $n$ full levels and $n + 1$ half-levels. The $z_\rho$ levels are positioned approximately half way between the $z_w$ levels.

## 4. Steady-state equations and methodology

In order to obtain a steady state for which the effects of vertical discretisation can be examined, it is sufficient to consider a one-dimensional column model by neglecting horizontal dependency. It is also assumed that reference vertical velocity is negligible, meaning the horizontal pressure gradients are independent of height and may be replaced by their free atmosphere value. Using these approximations, terms in Eqs (1)–(5) are expanded into steady and transient parts, e.g. $u = u^{(\mathrm{r})} + u'$; superscript (r) is used to denote the steady part and superscript $'$ is used to denote the transient part. The steady-state equations are obtained by ignoring any terms containing transients:

$$0 = f\left(v^{(\mathrm{r})} - v_{\mathrm{g}}\right) + \frac{1}{\rho^{(\mathrm{r})}}\frac{\partial}{\partial z}\left(\rho^{(\mathrm{r})}\tau_x^{(\mathrm{r})}\right), \tag{25}$$

$$0 = -f\left(u^{(\mathrm{r})} - u_{\mathrm{g}}\right) + \frac{1}{\rho^{(\mathrm{r})}}\frac{\partial}{\partial z}\left(\rho^{(\mathrm{r})}\tau_y^{(\mathrm{r})}\right), \tag{26}$$

$$0 = -c_p\theta^{(\mathrm{r})}\frac{\partial \pi^{(\mathrm{r})}}{\partial z} - g, \tag{27}$$

$$0 = \frac{1}{\rho^{(\mathrm{r})}}\frac{\partial}{\partial z}\left(\rho^{(\mathrm{r})}\mathcal{H}^{(\mathrm{r})}\right). \tag{28}$$

Note that the steady-state version of Eq. (5) is zero on both sides and so is omitted.

The surface boundary conditions for the velocities and potential temperature are

$$u^{(\mathrm{r})} = v^{(\mathrm{r})} = w^{(\mathrm{r})} = 0 \qquad \text{at} \quad z = z_{\mathrm{r}}, \tag{29}$$

$$\theta^{(\mathrm{r})} = \theta_s \qquad \text{at} \quad z = z_{\mathrm{r}}. \tag{30}$$

At the top of the domain, the boundary conditions are

$$u^{(\mathrm{r})} = v^{(\mathrm{r})} = u_{\mathrm{g}}, \;\; w^{(\mathrm{r})} = 0\,\mathrm{m\,s^{-1}} \qquad \text{at} \quad z = d, \tag{31}$$

$$\theta^{(\mathrm{r})} = 308\,\mathrm{K} \qquad \text{at} \quad z = d. \tag{32}$$

Values $u_{\mathrm{g}}$, $v_{\mathrm{g}}$ and $\theta_s$ are altered to give a range of cases of boundary-layer depth.

The steady-state solution is determined iteratively (see below). Where required, the density is obtained from the latest estimate of potential temperature as follows. Rearranging Eq. (27) gives

$$\pi^{(\mathrm{r})}(z) = -\int_{z_{\mathrm{r}}}^{d} \frac{g}{c_p\theta^{(\mathrm{r})}}\,\mathrm{d}z. \tag{33}$$

Using $\theta^{(\mathrm{r})}$, Exner pressure $\pi^{(\mathrm{r})}$ is obtained by evaluating Eq. (33). Pressure $p^{(\mathrm{r})}$ can be obtained from $\pi^{(\mathrm{r})}$ using Eq. (8) and then density can be obtained using Eq. (7). A realistic surface pressure is $p_s = 1000$ hPa; in order to obtain a value close to this at the surface, the pressure at the top of the domain is chosen to be $p_{\mathrm{g}} = 810$ hPa.

Note that, since a gradient of potential temperature is required at the same level as Exner pressure for the above calculation, the Lorenz grid will involve some averaging.

### 4.1. Using subsidence to balance diffusion

In their current form, it would not be possible to obtain a steady-state solution of Eqs (25)–(28) that supports a realistic potential temperature profile. The diffusion in the equation is unbalanced resulting in cooling of the boundary layer to the surface potential temperature. To balance this cooling, a subsidence heating is introduced; this allows for a realistic profile to be obtained while also allowing a steady state to be reached. Subsidence warming in boundary layers has been identified in very stable Antarctic atmospheric boundary layers (Mirocha and Kosovic, 2010). The subsidence warming is included by reintroducing the vertical advection term in the potential temperature equation but with an imposed velocity,

$$w_{\mathrm{sub}}\frac{\partial \theta^{(\mathrm{r})}}{\partial z}. \tag{34}$$

A form for the imposed subsidence velocity $w_{\mathrm{sub}}$ that produces a realistic potential temperature profile is found empirically and given by

$$w_{\mathrm{sub}} = -0.015\tanh\left(\frac{z}{z_{\mathrm{sub}}}\right), \tag{35}$$

where $z_{\mathrm{sub}} = 1000$ m.

In addition to the subsidence warming, a radiative cooling $R_{\mathrm{c}}$ is also included to ensure stable stratification throughout the domain. Neutral stratification above the boundary layer may result in a spurious nocturnal jet-type effect, meaning a steady state could not be reached. The rate of radiative cooling is chosen as $1\,\mathrm{K\,day^{-1}}$, which has only a small effect on the temperature in the boundary layer. With the addition of the subsidence warming and radiative cooling, Eq. (28) becomes

$$0 = -\frac{1}{\rho^{(\mathrm{r})}}\frac{\partial}{\partial z}\left(\rho^{(\mathrm{r})}\mathcal{H}^{(\mathrm{r})}\right) - w_{\mathrm{sub}}\frac{\partial \theta^{(\mathrm{r})}}{\partial z} - R_{\mathrm{c}}. \tag{36}$$

Note that, for stability, $\partial\theta^{(\mathrm{r})}/\partial z$ is computed using an upwind approximation.

### 4.2. Transformation to logarithmic coordinate

No general analytical solution of Eqs (25)–(27) and (36) is available, and so the Lorenz and Charney–Phillips grids at operational resolution are compared to a high-resolution reference solution. The number of grid points used in the high-resolution simulation should be sufficient, so that there is no discernible difference between the Lorenz and Charney–Phillips grids. In order for this to be achieved for a relatively small number of grid points requires that the system exhibits good convergence with resolution.

It is well known that, near the surface, model variables have mean properties proportional to the log of their distance from the wall (Holton, 2004). For example, the logarithmic wind speed profile is given by $u \sim \ln(z/z_{\mathrm{r}})$. In this regime, the vertical derivative approaches a singularity as $z \to 0$. Consequently numerical solutions do not converge until grid spacing is comparable to the roughness length.

In order to get around the singularity, one can perform a transformation to a logarithmic coordinate $\zeta = \zeta(z)$, as in Beljaars *et al.* (1987) and Weng and Taylor (2003). For any model variable whose derivative is required, the chain rule is applied to obtain, for example,

$$\frac{\partial u}{\partial z} = \frac{\partial \zeta}{\partial z}\frac{\partial u}{\partial \zeta}. \tag{37}$$

Now, provided that $\zeta(z) \to \ln(z)$ as $z \to 0$, it is found that, near to the ground,

$$\frac{\partial u}{\partial z} = \frac{1}{z}\frac{\partial u}{\partial \zeta}, \tag{38}$$

where $\partial u/\partial\zeta$ is a bounded derivative. Further, there is now a convenient cancelling of $z$ in $K_\mathrm{m}$ and $K_\mathrm{h}$ close to the ground, limiting the singularity. All high-resolution solutions shown are computed using the logarithmic coordinate and can be considered to have been computed using either the Lorenz grid or Charney–Phillips grid. Here the hybrid log-linear grid spacing employed by Weng and Taylor (2003) is used,

$$\zeta = \ln\left(\frac{z+z_\mathrm{r}}{z_\mathrm{r}}\right) + \frac{z}{z_\zeta}, \tag{39}$$

where $z_\zeta = 67.5$ m. Using the hybrid coordinate gives good resolution near the top of the boundary layer while also giving good convergence properties. All high-resolution solutions can be considered to have been computed using either the Lorenz grid or the Charney–Phillips grid.

For operational resolution simulations, a false time-stepping scheme is implemented, i.e. an iteration which includes the temporal derivative but assumes that all transient behaviour will decay or have negligible growth. For the false time-stepping scheme, stability is approximately governed by $K\Delta t/\Delta z^2 < 1$, sometimes known as the viscous Courant number. When a high-resolution logarithmic grid is implemented, the condition for stability would result in an exceptionally small time step, meaning simulations could not be run within a sensible time frame. Instead of false time-stepping the Newton method is implemented; the steady state is the root of the equations. The Newton method has been compared with false time-stepping for a range of neutral boundary layers and is found to be robust in approaching the proper steady state.

Due to the strong nonlinearities in the full stable boundary-layer equations, the Newton iteration quickly diverges if only a naïve guess for the solution is used to initialise the iteration. The following modification of the Newton method is found to provide good convergence. A multiplicative factor is placed in front of the stability functions; it is initially set to zero but gradually increased to one as the Newton iterations proceed. As well as being fast, the Newton method has the added advantage that the Jacobian of the system is computed, which is also used in the transient part of the study in Part II.

## 5. Steady-state results

Using the high-resolution logarithmic grid solution as a reference, the Lorenz grid is compared with the Charney–Phillips grid. Due to the choices present for the Charney–Phillips grid, there are a large number of results. The comparison is split by the three general options for the averaging when using the Charney–Phillips grid, options I, II and III. The number of required tests is further enlarged by the need to perform the comparison for a range of boundary-layer depths. In all there are fifteen Charney–Phillips configurations and one Lorenz configuration across five boundary-layer depths, making for eighty cases to consider. Since a large number of cases have been considered, only the most informative results are explicitly presented; Holdaway (2010) gives a more comprehensive presentation of results. The boundary-layer depths which will be used for the testing here are outlined in Table 1.

Table 1. Five boundary layers with varying depths, dependent on the boundary conditions of velocities and potential temperature.

| Notation | $u_g, v_g$ (m s$^{-1}$) | $\theta_s$ (K) | Approx. depth (m) |
|---|---|---|---|
| BL1 | 4 | 283 | 100 |
| BL2 | 6 | 288 | 200 |
| BL3 | 8.5 | 293 | 400 |
| BL4 | 10.5 | 298 | 650 |
| BL5 | 14 | 298 | 950 |

### 5.1. *Charney–Phillips grid option I configurations*

The first comparison is between the high-resolution solution, the Lorenz grid solution and the Charney–Phillips grid option I solutions. For option I configurations, Richardson number is computed at $z_w$ levels and there are i-iii sub-options for how $K_\mathrm{h}$ is obtained. The averaging steps taken to obtain $K_\mathrm{m}$ and $K_\mathrm{h}$ at their relevant levels are shown in Figure 2.

The comparison between high-resolution grid, Lorenz grid, and Charney–Phillips grid option I-i to I-iii configurations is shown in Figures 3 and 4, the former showing the $u^{(\mathrm{r})}$ and $v^{(\mathrm{r})}$ velocity field components, and the latter the potential temperature $\theta^{(\mathrm{r})}$ and density $\rho^{(\mathrm{r})}$ fields.

Firstly it should be noted that all of the four low-resolution configurations perform reasonably well. No configuration has an issue in predicting the general structure of the boundary layer and none is particularly far from the high-resolution solution.

In the cases examined here, there is found to be little benefit to the Charney–Phillips grid option I-ii configuration. For the range of boundary-layer depths tested, it is almost always less accurate than the I-i and I-iii configurations, except at the level closest to the ground. For the level closest to the ground, the option I-ii configuration is the most accurate of the three Charney–Phillips configurations. However it is not so significantly better than the other Charney–Phillips configurations to warrant sacrificing accuracy higher in the boundary layer to gain extra accuracy close to the surface. The option I-ii configuration does particularly poorly in predicting the potential temperature field.

In the upper part of the boundary layer, the Charney–Phillips grid option I-i and I-iii configurations perform most accurately. For the potential temperature field at the very top of the boundary layer, the Charney–Phillips option I-iii grid clearly produces the most accurate solution, followed by the Lorenz and Charney–Phillips option I-i grids, which produce similar levels of accuracy. For the velocity fields at the very top of the boundary layer, the Charney–Phillips option I-iii grid is also the most accurate and the Charney–Phillips grid option I-i configuration is more accurate than the Lorenz grid.

Although the Lorenz grid is less accurate than the Charney–Phillips option I-i and I-iii configurations for the upper part of the boundary layer, it is often more accurate for the grid points nearest the surface. For the $v^{(\mathrm{r})}$ component of velocity and for the potential temperature

 

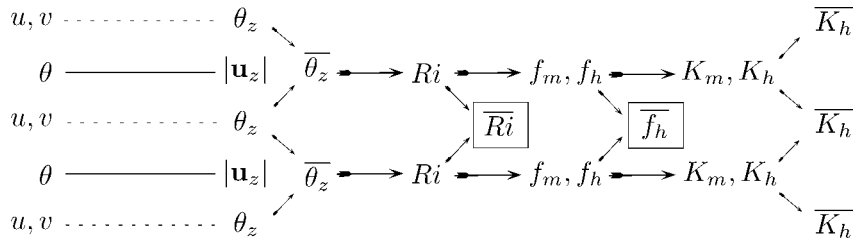


**Figure 2.** The steps taken to obtain $K_m$ and $K_h$ with the Charney–Phillips grid option I configurations on a section of the grid away from boundaries. The option I-ii and I-iii choices are shown in the boxes.

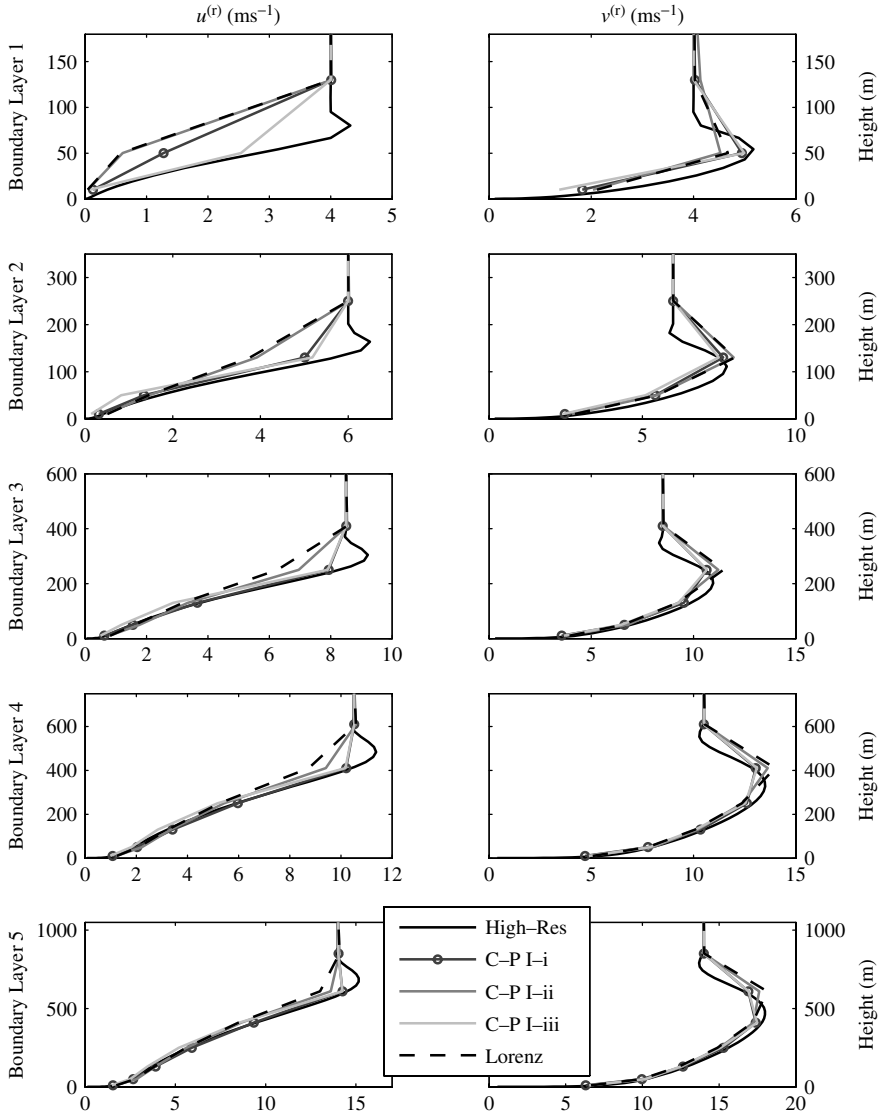


**Figure 3.** Comparison of steady states found using the Lorenz and Charney–Phillips grid option I configurations. This shows the $u^{(r)}$ and $v^{(r)}$ profiles. From top to bottom are the results for boundary layer 1 to boundary layer 5.

$\theta^{(r)}$, the Lorenz grid is the most accurate near the surface for all the boundary-layer depths examined, and for the deepest boundary layers tested the Lorenz grid outperforms the Charney–Phillips grid configurations for the lowest two grid points in the potential temperature field. However, for the $u^{(r)}$ component of the velocity either the option I-i or I-iii Charney–Phillips grid configurations produces the most accurate solution for all grid points and all boundary-layer depths.

For the density field there is less to distinguish between the different grids. For the deepest boundary layers all four configurations capture the structure accurately and near the surface they all give very close values. For the shallow boundary layers the Charney–Phillips option I-iii configuration can again be seen to be doing well at the top of the boundary layer. The Lorenz grid also performs well near the top of the boundary layer. Nearer to the surface it is the Charney–Phillips option I-i and I-iii configurations that produce the most accurate results.

The Charney–Phillips option I-i configuration is the best all-rounder. Although it does not have the benefit of being consistently the most accurate grid for a certain region of

 

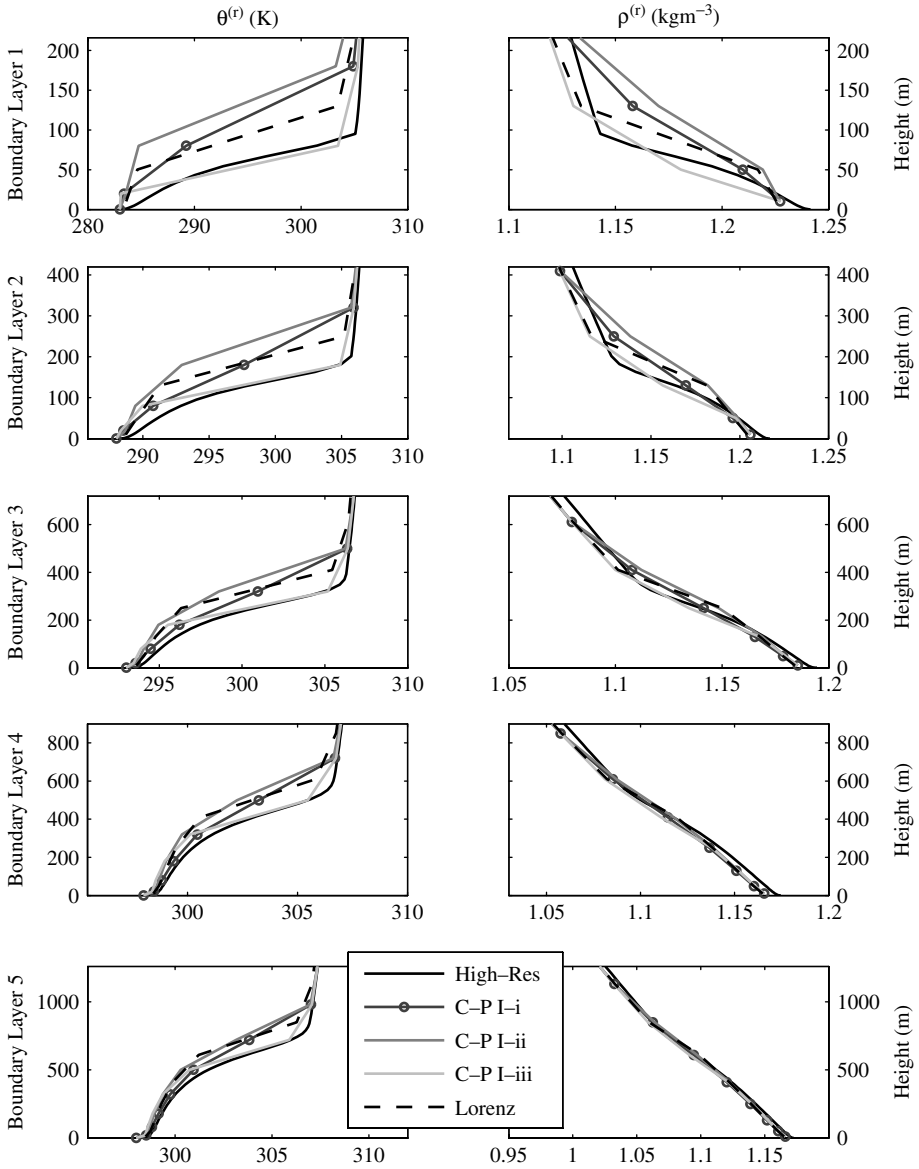


**Figure 4.** As Figure 3, but showing the $\theta^{(r)}$ and $\rho^{(r)}$ profiles.

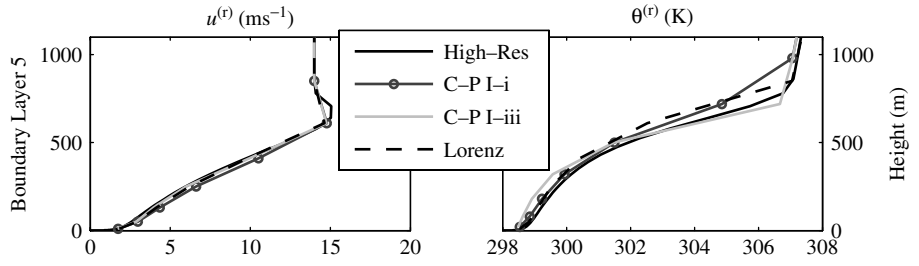


**Figure 5.** Comparison of the Lorenz grid and Charney–Phillips grid option I-i and I-iii configurations for the boundary layer only. The left plots show the $u^{(r)}$ component of velocity and the right plots show $\theta^{(r)}$. The boundary-layer case is displayed on the $y$-axis.

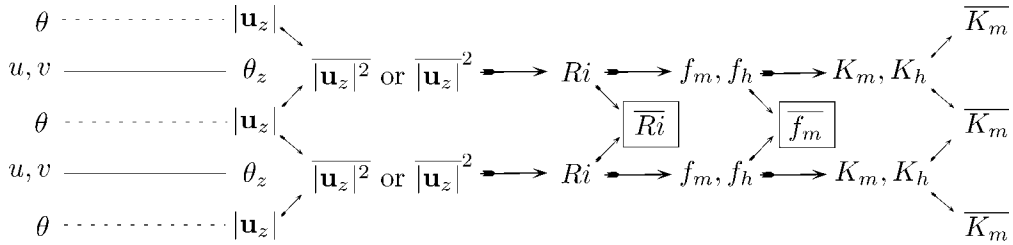


**Figure 6.** As Figure 2, but for the Charney–Phillips grid option II configurations. The beginning of the alternative options for finding $K_m$ are shown in the boxes.

 

the boundary layer, it tends to produce results close the best grid at all points. Based on the steady-state results, it seems likely that the option I-i configuration would offer the best option for use in models of this kind.

If certain dynamics are ignored by making a Boussinesq approximation, meaning that density is constant in the solution, the Lorenz grid would be expected to produce the most accurate results as it would eliminate all averaging. Figure 5 shows the $u^{(r)}$ component of velocity and the potential temperature for the Lorenz grid and Charney–Phillips grid option I-i and I-iii configurations when solving the boundary layer-only case. The case shown is boundary layer 5.

For the Boussinesq boundary layer-only case, the Lorenz grid gives the most accurate results for all grid points for the velocity fields (only $u^{(r)}$ shown). This is also the case for the shallower boundary layers. The potential temperature field is also captured significantly more accurately by the Lorenz grid once the density is excluded. For the case presented, there is still one grid point for which the Charney–Phillips option I-iii configuration does better than the Lorenz grid, however the difference is considerably smaller than for the coupled case. For other boundary-layer depths, the difference between the grids has been found to be even less. It must be noted that results are found to be somewhat dependent on the location of grid points and how well they coincide with certain features, such as the location of the top of the boundary layer.

It is interesting to note that the required averaging in the hydrostatic balance step can damage the Lorenz grid steady-state solution to the point that it is no longer the preferred overall grid. It is also the averaging in this term that leads to the poor Lorenz grid behaviour witnessed by Thuburn and Woollings (2005) and Thuburn (2006). Despite the Charney–Phillips configurations having averaging of the boundary-layer terms and the Lorenz grid having no averaging, situations arise when the Charney–Phillips grid can be more accurate, emphasising the need for careful analysis over heuristic arguments for grid selection.

### 5.2. *Charney–Phillips grid option II configurations*

The second set of tests covers the Charney–Phillips grid option II configurations; for these the Richardson number is computed at the velocity levels and so $K_h$ rather than $K_m$ is obtained automatically. Option II has the largest number of potential configurations since there are options for how to compute the shear and under these there are also the similar options to those that occur under option I for how to compute $K_m$. Figure 6 shows a selection from the possible steps that are required in order to obtain $K_m$ and $K_h$ when using option II.

Figure 7 shows the high-resolution and Charney–Phillips grid option II(b)-i and II(c)-iii configuration solutions for boundary layers 1, 3 and 5. Clearly the inaccuracy introduced by this choice of averaging prevents a sensible solution from being formed.

Both of the Charney–Phillips grid solutions in Figure 7 develop significant discontinuities in the solution. These discontinuities can lead to additional nocturnal jet-like behaviour as velocity is continuously introduced spuriously above the boundary layer and where there is no diffusion to suppress it. When a spurious nocturnal jet effect is introduced, it leads to additional rotation in the wind above the boundary layer. As a result, those simulations had to be halted as they would not approach steady state. There are a total of nine Charney–Phillips grid option II configurations examined here. All were found to encounter problems which lead to discontinuities in the steady-state solution or failure to generate a steady state. It is found that the inaccuracies in the solution do not depend on whether the hydrostatic dynamics are included; large discontinuities in the solution are found for both the fully compressible and Boussinesq equation models.

It is difficult to identify the exact source of the large errors seen in the solution since they occur very quickly during the simulation. Usually within five or fewer iterations large discontinuities are evident. After a couple of iterations, a large spike is evident near the surface in the Richardson number field and by the next iteration the model variables have large discontinuities. Errors appear to be independent of the numerical scheme that is used; both false time-stepping and the Newton method have been tested at varying resolutions and for different types of grid stretching, and all simulations resulted in similar problems. The large errors seen for this case are discussed further in section 5.4.

### 5.3. *Charney–Phillips grid option III configurations*

The final set of testing is for the Charney–Phillips grid option III configurations. Option III configurations average both potential temperature and velocity gradients so that Richardson number is computed at all model levels, no suboptions i–iii are necessary, however the options (a)–(c) still exist for computing the averaged shear. The steps taken for options III(b) and III(c) are shown in Figure 8.

Figure 9 shows the high-resolution and Charney-Phillips grid option III(b) and III(c) configuration solutions for boundary layer 5. Again it can be seen that the averaging is introducing an inaccuracy into the solution. There are clear discontinuities in the potential temperature field. Although problems occur with the option III configurations, they are less severe than the problems seen with the option II configurations. There are discontinuities in the potential temperature fields but the wind field solutions are fairly accurate, although not as accurate as the solution given by the option I configurations.

### 5.4. *Problems with the Charney–Phillips grid when using options II and III: Interpretation*

Clearly there is a degree of sensitivity to any error that occurs during averaging of shear that is causing inaccuracy in the Charney–Phillips grid option II and III solutions. Fortunately the model is less sensitive to inaccuracy introduced when averaging the potential temperature gradient and so useful solutions, using Charney–Phillips grid option I, are possible. That the errors are caused by sensitivity to inaccuracy attained when averaging shear is ratified by finding errors in option III to be less significant. Comparing options II and III, there is a significant difference between the way the averaged shear interacts with the model variables. When using option II, both $K_m$ and $K_h$ are evaluated using averaged shear. When using option III, $K_h$ is calculated using averaged shear while $K_m$ is calculated using averaged potential temperature gradient. The option III configuration can be considered a combination of options I and II: velocity is updated via an option I-type scheme

 

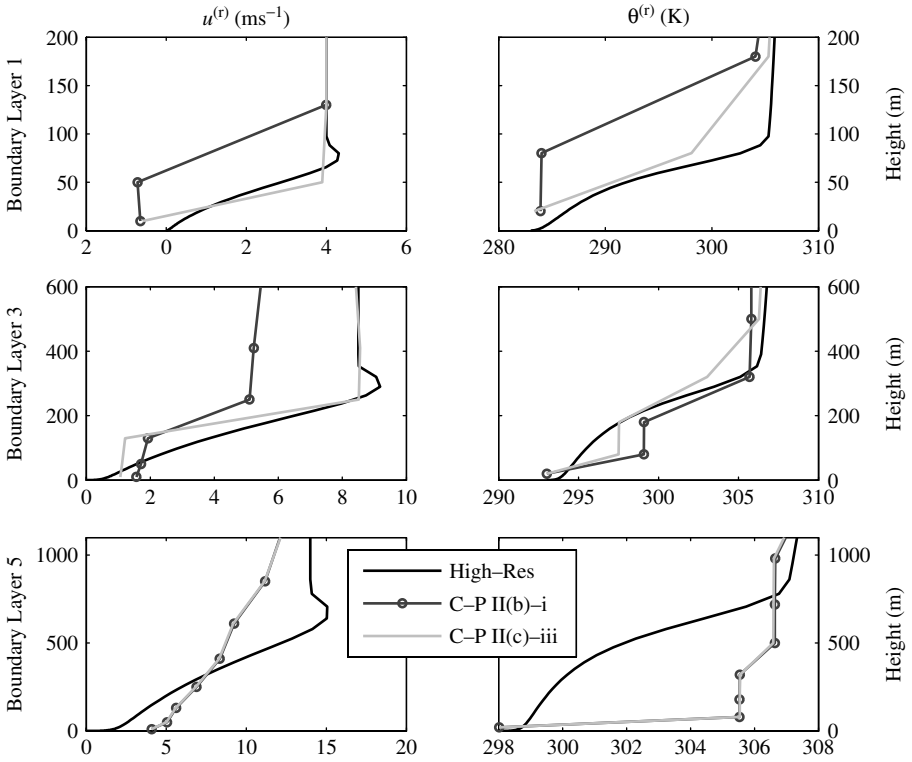


**Figure 7.** As Figure 5, but comparing high resolution with options II(b)-i and II(c)-iii configurations.

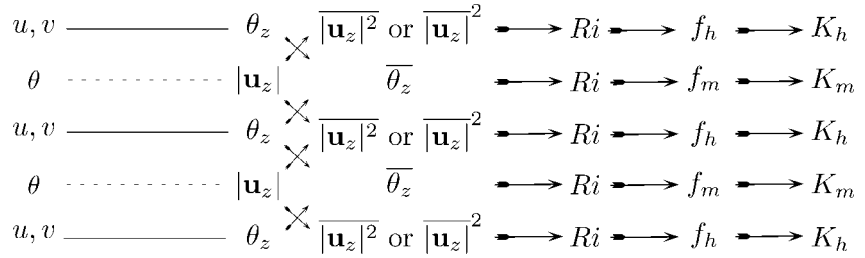


**Figure 8.** As Figure 2, but for the option III(b) and III(c) grids.

and potential temperature by an option II-type scheme. As a result, the potential temperature field has large errors but the velocity field does not. Figures 10 and 11 show schematically the flow of information and feedbacks between key variables during the time step update for the option II and III configurations, respectively.

When using option II (Figure 10), the averaged shear enters the Richardson number, which then enters the stability function and the eddy viscosity and diffusivity. Also, the averaged shear is used directly in the eddy viscosity and diffusivity (option II(a–c)-i). When using option III (Figure 11), the averaged shear only enters the Richardson number on the potential temperature side of the loop. The only way the averaged shear interacts with the velocity again is by passing through the potential temperature into the averaged potential temperature gradient. As the averaged shear quantity passes through the potential temperature side of the loop and then the velocity side of the loop, it is likely that any error will be smoothed out and its impact reduced. When using option II, the averaged shear is used to update velocity more directly, producing errors in the velocity which will in turn produce even greater errors in the shear. The errors quickly produce a feedback and within a few time steps the model solution deteriorates. It is interesting to note that, for option III, the step-like features in potential temperature do not result in large errors in the velocities.

A number of experiments were devised in order to eliminate the possibility that the poor performance of the option II and III configurations is simply due to some numerical artefact. As discussed above, both false time stepping and the Newton method were used for grids with different stretching factors. The model was also initialised in a range of different ways, including with a solution obtained using Charney–Phillips grid option I.

It is well known that nonlinear mixing or diffusion can, under certain circumstances, produce step-like features in the mixed variable. This happens when the local rate of mixing increases as the gradient of the mixed quantity decreases; this results in a positive feedback that leads to localized well-mixed regions separated by sharp gradients. For vertical mixing in stratified fluids, this phenomenon is known as the 'Phillips Effect' (Phillips, 1972). A similar effect occurs in the quasi-horizontal mixing of potential vorticity (Dritschel and McIntyre, 2008) and is thought to play a role in the maintenance of Jupiter's jets as well as sharpening the subtropical tropopause and the edge of the stratospheric winter vortex. These ideas, together with the feedbacks

 

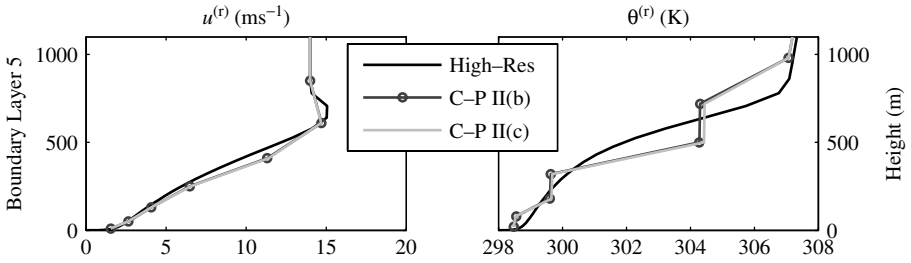


**Figure 9.** As Figure 5, but comparing high resolution with option III(b) and III(c) configurations.

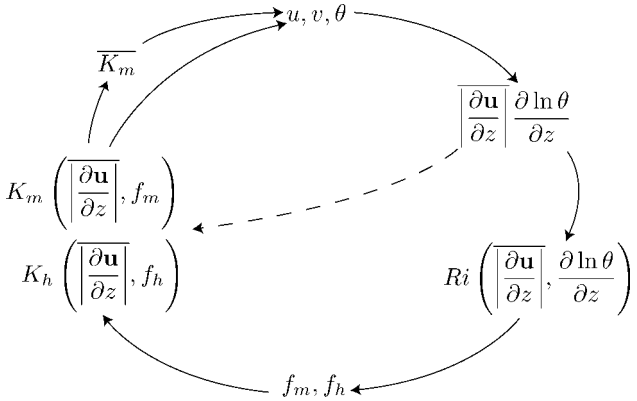


**Figure 10.** Flow diagram demonstrating the process of updating the model variables during iteration using Charney–Phillips grid option II(b)-i.

depicted in Figures 10 and 11, suggest the following explanation for the behaviour of the configurations studied here.

The dependence of $K_\mathrm{m}$ and $K_\mathrm{h}$ on the gradient of potential temperature provides a Phillips Effect positive feedback. At the same time, at least for the continuous boundary-layer model of section 2 and the successful Lorenz and Charney–Phillips option I configurations, the dependence on the shear produces a negative feedback. For the stable boundary layer, the negative feedback dominates, leading to smooth boundary-layer profiles (except perhaps at the very top of the boundary layer). However, for the Charney–Phillips option II and III configurations, the averaging of the shear suppresses the negative feedback, allowing the positive feedback to dominate and step-like features to form.

The effect of the feedbacks is demonstrated in Figure 12. Here the Lorenz grid solution is iterated but with the updating of velocity switched off. The initial conditions are the steady-state profiles previously found but with a random small perturbation to the potential temperature profile in the boundary layer. Holding the velocity side of the iteration constant prevents the negative feedback and allows the perturbation to potential temperature to grow and form steps. Profiles for $\theta^{(\mathrm{r})}$ are plotted after 0, 1000, 5000 and 25 000 iterations; the step structure is evident. If the velocity updating is then reinstated, the solution returns to the proper steady state.

In order to keep the number of cases manageable, only centred second-order finite-differencing has been examined here. It might be wondered whether the use of higher-order numerics would affect the conclusions. The poor behaviour of the Charney–Phillips option II and option III configurations results from vertical averaging of shear terms. That vertical averaging cannot be avoided, and its effect would be similar even if a higher-order vertical averaging were used, or if higher-order numerics were used for other terms. Therefore we anticipate that options II and III would remain poorly behaved even for higher-order numerics.

## 6. Conclusions

In this study, the ability of the Lorenz and Charney–Phillips vertical grid staggering techniques are compared for solving a model of dynamics coupled to the planetary boundary layer. In this Part I of the study, the Lorenz and Charney–Phillips grids have been compared for capturing the steady state of the model. This has been a non-trivial exercise due to the complexities involved in the nonlinear equations. A subsidence heating and radiative cooling had to be introduced in order that the model could reproduce a realistic profile for the potential temperature. Further, the logarithmic behaviour close the ground led to issues in obtaining a suitably converged high-resolution reference solution. This issue was rectified by performing a transition to a logarithmic coordinate and then using the Newton method so as to ensure that computational cost was not prohibitive.

In computing the steady state, it was shown that the Lorenz grid is preferred for capturing the solution when only the boundary layer is represented; this is as expected since eliminating enough dynamics also eliminates any need for averaging when using the Lorenz grid. However there can be grid points for which a Charney–Phillips configuration can produce more accurate results than the Lorenz grid.

When dynamics are included, through the hydrostatic balance, it is generally the Charney–Phillips grid that produces the most accurate overall results, despite the required averaging in the boundary-layer terms. However there is no overall 'optimal' configuration. The Charney–Phillips grids which give the most accurate results are those that involve the averaging of only the potential temperature gradient. Charney–Phillips configurations that involve averaging of shear all produce solutions with significant non-physical steps due to the suppression of a negative feedback that results from averaging of shear.

The results demonstrate how closer analysis of the configurations, as opposed to basing a grid choice on heuristic arguments, can be useful. It would be difficult to predict that the Charney–Phillips grid would outperform the Lorenz grid in the boundary-layer region, given that the only averaging for the Lorenz grid is in the hydrostatic balance step. Also, when the Boussinesq approximation is made and there is no averaging for the Lorenz grid, the Charney–Phillips grid can still produce comparable results, particularly near the top of the boundary layer. Further it is not immediately obvious that certain Charney–Phillips

 

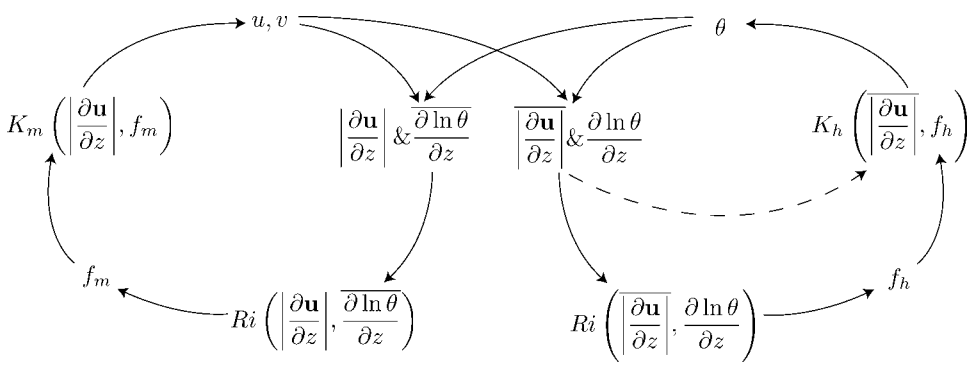


**Figure 11.** Flow diagram demonstrating the process of updating the model variables during iteration using Charney–Phillips grid option III(b).

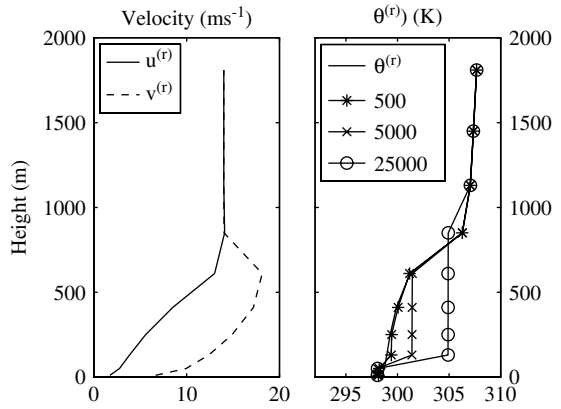


**Figure 12.** The evolution of $\theta^{(r)}$ using the Lorenz grid and with the initial conditions set to the steady state, but with a small random perturbation added. Throughout the iteration, velocities are fixed at their steady state. Potential temperature is shown after 500, 5000 and 25 000 iterations.

configurations should perform well while others are problematic.

In computing the steady states, differences between the Lorenz and Charney–Phillips grids and problems with certain Charney–Phillips configurations have been identified. Schemes resulting in solutions with large steps are not recommended. Although the steady-state study is useful, it is important also to consider the handling of the time-dependent evolution of the model and this is the subject of Part II of this study.

## Acknowledgements

The lead author wishes to thank the EPSRC and the Met Office for funding this work under an Industrial CASE partnership. Further thanks are due to the dynamics research group at the Met Office for providing access to their expertise.

## References

Arakawa A, Konor CS. 1996. Vertical differencing of the primitive equations based on the Charney–Phillips grid in hybrid $\sigma - p$ vertical coordinates. *Mon. Weather Rev.* **124**: 511–528.

Arakawa A, Lamb VR. 1977. Computational design of the basic dynamical processes of the UCLA general circulation model. *Methods Comput. Phys.* **17**: 173–265.

Arakawa A, Moorthi S. 1988. Baroclinic instability in vertically discrete systems. *J. Atmos. Sci.* **45**: 1688–1708.

Beljaars ACM. 1992. 'The parametrization of the planetary boundary layer'. Lecture notes, ECMWF: Reading, UK. Available at http://www.ecmwf.int/newsevents/training/lecture_notes/LN_PA.html

Beljaars ACM, Walmsley JL, Taylor PA. 1987. A mixed spectral finite-difference model for neutrally stratified boundary-layer flow over roughness changes and topography. *Boundary-Layer Meteorol.* **38**: 273–303.

Charney JG, Phillips NA. 1953. Numerical integration of the quasi-geostrophic equations for barotropic and simple baroclinic flows. *J. Meteorol.* **10**: 71–99.

Cullen MJP, Salmond DJ. 2003. On the use of a predictor–corrector scheme to couple the dynamics with the physical parametrizations in the ECMWF model. *Q. J. R. Meteorol. Soc.* **129**: 1217–1236.

Cullen MJP, Davies T, Mawson MH, James JA, Coulter SC, Malcolm A. 1997. An overview of numerical methods for the next generation UK NWP and climate model. In *Numerical Methods in Atmosphere and Ocean Modelling; The André J. Robert memorial volume*, Lin C, Laprise R, Ritchie H. (eds) Canadian Meteorol. Oceanogr. Soc: 425–444.

Davies T, Cullen MJP, Malcolm A, Mawson MH, Staniforth A, White AA, Wood N. 2005. A new dynamical core for the Met Office's global and regional modelling of the atmosphere. *Q. J. R. Meteorol. Soc.* **131**: 1759–1782.

Dritschel DG, McIntyre ME. 2008. Multiple jets as PV staircases: The Phillips effect and the resilience of eddy-transport barriers. *J. Atmos. Sci.* **65**: 855–874.

Dubal M, Wood N, Staniforth A. 2004. Analysis of parallel versus sequential splittings for time-stepping physical parameterizations. *Mon. Weather Rev.* **132**: 121–132.

Dubal M, Wood N, Staniforth A. 2005. Mixed parallel-sequential-split schemes for time-stepping multiple physical parameterizations. *Mon. Weather Rev.* **133**: 989–1002.

Dubal M, Wood N, Staniforth A. 2006. Some numerical properties of approaches to physics–dynamics coupling for NWP. *Q. J. R. Meteorol. Soc.* **132**: 27–42.

Fox-Rabinovitz MS. 1994. Computational dispersion properties of vertically staggered grids for atmospheric models. *Mon. Weather Rev.* **122**: 377–392.

Holdaway D. 2010. 'Coupling the planetary boundary layer to the large-scale dynamics of the atmosphere: The impact of vertical discretisation'. PhD thesis. University of Exeter: Exeter, UK.

Holdaway D, Thuburn J, Wood N. 2012. Comparison of Lorenz and Charney–Phillips vertical discretisations for dynamics–boundary layer coupling. Part II: Transients. *Q. J. R. Meteorol. Soc.* DOI: 10.1002/qj.2017.

Hollingsworth A. 1995. 'A spurious mode in the 'Lorenz' arrangement of $\Phi$ and $T$ which does not exist in the 'Charney–Phillips' arrangement'. Tech. Memo. 211. ECMWF: Reading, UK.

Holton JR. 2004. *An Introduction to Dynamic Meteorology*. *Internat. Geophys.* Series **88**: Elsevier Academic Press.

King JC, Conolley WM, Derbyshire SH. 2001. Sensitivity of modelled Antarctic climate to surface and boundary-layer flux parametrizations. *Q. J. R. Meteorol. Soc.* **127**: 779–794.

Lorenz EN. 1960. Energy and numerical weather prediction. *Tellus* **12**: 364–373.

Louis J-F. 1979. A parametric model of vertical eddy fluxes in the atmosphere. *Boundary-Layer Meteorol.* **17**: 187–202.

Mirocha JD, Kosovic B. 2010. A large-eddy simulation study of the influence of subsidence on the stably stratified atmospheric boundary layer. *Boundary-Layer Meteorol.* **134**: 1–21.

Phillips OM. 1972. Turbulence in a strongly stratified fluid – is it unstable? *Deep-Sea Res.* **19**: 79–81.

 

Schneider EK. 1987. An inconsistency in vertical discretization in some atmospheric models. *Mon. Weather Rev.* **115**: 2166–2169.

Staniforth A, Wood N, Côté J. 2002a. Analysis of the numerics of physics–dynamics coupling. *Q. J. R. Meteorol. Soc.* **128**: 2779–2799.

Staniforth A, Wood N, Côté J. 2002b. A simple comparison of four physics–dynamics coupling schemes. *Mon. Weather Rev.* **130**: 3129–3135.

Tannehill JC, Anderson DA, Pletcher RH. 1997. *Computational Fluid Mechanics and Heat Transfer*. Taylor and Francis.

Thuburn J. 2006. Vertical discretizations giving optimal representation of normal modes: Sensitivity to the form of the pressure-gradient term. *Q. J. R. Meteorol. Soc.* **132**: 2809–2825.

Thuburn J, Woollings T. 2005. Vertical discretizations for compressible Euler equation atmospheric models giving optimal representation of normal modes. *J. Comput. Phys.* **203**: 386–404.

Toy MD, Randall DA. 2007. Comment on the article 'Vertical discretizations for compressible Euler equation atmospheric models giving optimal representation of normal modes'. *J. Comput. Phys.* **223**: 82–88.

Untch A, Hortal M. 2004. A finite-element scheme for the vertical discretization of the semi-Lagrangian version of the ECMWF forecast model. *Q. J. R. Meteorol. Soc.* **130**: 1505–1530.

Wedi NP. 1999. 'The numerical coupling of the physical parametrizations to the 'dynamical' equations in a forecast model'. Tech. Memo. 274, ECMWF: Reading, UK.

Weng W, Taylor PA. 2003. On modelling the one-dimensional atmospheric boundary layer. *Boundary-Layer Meteorol.* **107**: 371–400.

Williamson D. 2002. Time-split versus process-split coupling of parametrizations and dynamical core. *Mon. Weather Rev.* **130**: 2024–2041.

Zhu H, Smith RK. 2003. Effects of vertical differencing in a minimal hurricane model. *Q. J. R. Meteorol. Soc.* **129**: 1051–1069.

 